

1 **Temporal modulation of collective cell behavior controls vascular network topology**

2 Esther Kur¹, Jiha Kim¹, Aleksandra Tata¹, Cesar H. Comin², Kyle I Harrington³, Luciano
3 da F. Costa², Katie Bentley^{3,4}, Chenghua Gu^{1,4}

4

5 ¹ Department of Neurobiology, Harvard Medical School, 220 Longwood Ave, Boston,
6 MA 02115, U.S.A. ² IFSC, University of Sao Paulo, Sao Carlos, SP, Brazil. ³
7 Department of Pathology and Center for Vascular Biology Research, Beth Israel
8 Deaconess Medical Center, Harvard Medical School, 330 Brookline Avenue Boston, MA
9 02215 U.S.A

10

11

12

13

14 ⁴Correspondence and requests for materials should be addressed to

15 C.G. Chenghua Gu (chenghua_gu@hms.harvard.edu)

16 Department of Neurobiology, Harvard Medical School

17 Boston, MA 02115, U.S.A.

18 (Ph) 617-432-6364 (Fax) 617-432-1639

19 or

20

21 K.B. Katie Bentley (kbentley@bidmc.harvard.edu)

22 Computational Biology Lab, Center for Vascular Biology Research, Beth Israel Deaconess

23 Medical Center, Harvard Medical School, 220 Longwood Ave, Boston, MA 02115

24

25 **Completing Interests Statement**

26 The authors declare that no completing interests exist.

27

28 Vascular network density determines the amount of oxygen and nutrients delivered
29 to host tissues, but how the vast diversity of densities is generated is unknown.
30 Reiterations of endothelial-tip-cell selection, sprout extension and anastomosis are
31 the basis for vascular network generation, a process governed by the VEGF/Notch
32 feedback loop. Here, we find that *temporal* regulation of this feedback loop, a
33 previously unexplored dimension, is the key mechanism to determine vascular
34 density. Iterating between *computational* modeling and *in vivo* live imaging, we
35 demonstrate that the rate of tip-cell selection determines the length of linear sprout
36 extension at the expense of branching, dictating network density. We provide the
37 first example of a host tissue-derived signal (Semaphorin3E-Plexin-D1) that
38 accelerates tip cell selection rate, yielding a dense network. We propose that
39 *temporal* regulation of this critical, iterative aspect of network formation could be a
40 general mechanism, and additional temporal regulators may exist to sculpt vascular
41 topology.

42 The unique vascular topology of different organs exists for organ-specific functions.
43 Different vascular network densities determine the specific amount of oxygen and
44 nutrients to be delivered to each host tissue. Development of new vascular networks
45 depends upon two types of specialized endothelial cells that work together: (1) The
46 endothelial “tip cell”, which is located at the front of a growing vessel and guides its
47 extension by sensing and responding to environmental cues, analogous to the axonal
48 growth cone (Gerhardt et al., 2003; Kurz et al., 1996). (2) “Stalk cells”, which trail
49 behind the tip cell and elongate the sprout. Tip and stalk cell identities are primarily
50 controlled by the Dll4-Notch lateral inhibition pathway, which is activated in endothelial
51 cells in response to VEGF from the local environment. VEGF-induced Dll4 activates
52 Notch1 on the neighboring cell, leading to the down-regulation of VEGF receptor levels
53 (Figure 1B)(Hellström et al., 2007; Leslie et al., 2007; Lobov et al., 2007; Suchting et al.,
54 2007),(Benedito et al., 2009; Phng et al., 2009; Roca and Adams, 2007). Thus, lateral
55 inhibition between endothelial cells generates an alternating pattern of active tip cells
56 (Dll4 high) and inhibited stalk cells (Dll4 low). Moreover, tip cell selection is a dynamic
57 process, and tip cell identity is transient (Arima et al., 2011; Jakobsson et al., 2010).
58 Reiteration of tip cell selection, sprout extension, and connection of neighboring sprouts
59 (anastomosis) is the basis for building a sophisticated vascular network (Adams and
60 Eichmann, 2010; Carmeliet, 2000). Although this VEGF/Notch signaling pathway has
61 been well studied and found to be conserved among different vascular beds and species,
62 how this central pattern generator is modified by various target tissue-specific signals to
63 yield diverse network topologies is not known.

64 Here, we propose a general principle of how collective cell behavior determines the
65 diverse densities of different networks: the generation of vascular topologies depends
66 heavily on the *temporal* regulation of tip cell selection. Integrated simulations predict that
67 as cell neighborhoods change, due to anastomosis or cell rearrangement events, lateral
68 inhibition patterns will necessarily be disrupted, requiring continual re-selection of new
69 tip cells (Bentley et al., 2014a, 2009). In fact, mouse genetics experiments demonstrated
70 that tip cell numbers are positively correlated with the branching points of the network
71 (Hellström et al., 2007; Kim et al., 2011). Therefore, the *length of time* it takes to
72 establish (and re-establish) the alternating pattern of tip and stalk cells may be a missing,

73 critical determinant of vascular topology (Bentley et al., 2014b, 2014c). Here, we took an
74 integrated approach combining computational modeling, mouse genetics, and *in vivo*
75 endothelial cell tracking to determine whether tip/stalk patterning can be temporally
76 modulated to generate different topologies. We hypothesize that the frequency of tip cell
77 selection determines the length of linear extension vs. branching, thus dictating the
78 density of the network.

79

80 To begin to test this hypothesis, it is crucial to analyze dynamic single cell behavior and
81 collective movement in the context of network formation (Arima et al., 2011; Jakobsson
82 et al., 2010). Previously, we used static analyses of the postnatal mouse retina as a model
83 to understand how neural signals shape vascular topology (Kim et al., 2011). We
84 discovered that retina ganglion cell-derived Semaphorin3E (Sema3E) and its receptor
85 Plexin-D1, which is expressed in endothelial cells at the front of actively sprouting blood
86 vessels, control the VEGF/Notch pathway via a feedback mechanism. Mice lacking either
87 Sema3E or Plexin-D1 exhibited an uneven vascular growth front and a reduction of tip
88 cells that resulted in a less branched network compared to their wildtype littermate
89 controls (Kim et al., 2011) (Figure 1A). However, it is not clear how this phenotype is
90 generated: specifically, how the Sema3E-Plexin-D1 feedback mechanism regulates
91 VEGF/Notch signaling at a dynamic cellular level, and whether changes in temporal
92 modulation of this pathway lead to the overall vascular topology phenotype.

93

94 To begin to understand how Sema3E-Plexin-D1 signaling modifies vascular topology
95 formation in a dynamic, spatiotemporal manner, we took advantage of an existing agent-
96 based computational model (the “MemAgent-Spring Model” or MSM) that simulates the
97 cellular processes during tip cell selection making explicit the time it takes for gene
98 expression (e.g. transcription/translation) changes to occur (Figure 1B, C – note time
99 delay parameters D1 and D2) (Bentley et al., 2009, 2008). The MSM has been tested
100 against numerous independent experimental data sets and validated as predictive of new
101 mechanisms *in vivo/in vitro* (Bentley et al., 2014a; Guarani et al., 2011; Jakobsson et al.,
102 2010). To now simulate tip cell selection in the context of Sema3E-Plexin-D1 crosstalk
103 signaling with VEGF/Notch signaling (Fukushima et al., 2011; Kim et al., 2011) the

104 MSM model was extended by adding four new parameters (Figure 1B, Video 1-5), with
105 sensitivity analyses and calibration simulations performed, which include modulation of
106 the existing parameter (δ) representing the induction level of Dll4 by VEGFR-2
107 activation (See methods section). These four new parameters represent the time delay for
108 induction of Plexin-D1 by VEGF (D3), the time delay (D4) and strength (s) of the
109 reduction of Dll4 levels in response to Sema3E-Plexin-D1 signaling, based on the
110 experimental data previously shown (Kim et al., 2011), as well as the degradation rate of
111 Plexin-D1 (r_3). Loss of Sema3E-PlexinD1 signaling was simulated by setting all Plexin-
112 D1 levels to zero. Loss of function simulations recapitulated the two prominent features
113 of *Plxnd1*^{-/-} and *Sema3e*^{-/-} mutant retinal vasculature remarkably closely: *In vivo*, mutant
114 vascular networks exhibit fewer tip cells and 1.5-2 fold reduction in branching points, as
115 well as an uneven growth front (compare Figure 1A with 1C (red boxes)) (Kim et al.,
116 2011). Furthermore, the dynamic nature of the simulations provided a novel insight to
117 explain how this phenotype is generated. Simulations predict that higher Dll4 levels in
118 the cells generates a shift towards synchronized Dll4 fluctuations overtime in contiguous
119 cells, as they collectively battle more strongly via lateral inhibition negative feedback,
120 causing an overall delay in amplification of differences needed to select the alternating
121 pattern of tip and stalk cells (Figure 1C-E, Video 6,7). Therefore, computational
122 simulations suggest that Sema3E-Plexin-D1 signaling enhances the speed and frequency
123 of tip cell selection and thus increases the density of retinal vascular networks.

124

125 We next examined single cell behavior in a mosaic environment, because lateral
126 inhibition requires collective coordination, and the relative, not absolute, levels of Dll4
127 expression among neighboring cells determine the outcome of the tip cell selection
128 process (Jakobsson et al., 2010). A *Plxnd1*^{-/-} cell will behave differently in competition
129 with a second *Plxnd1*^{-/-} cell than in competition with a wildtype cell. Thus, we
130 investigated whether the cell autonomous function of Sema3E-Plexin-D1 signaling in the
131 direct competition process between two neighboring endothelial cells can drive changes
132 to the tip cell selection dynamics. In a simulated mosaic vessel, where cells lacking
133 Sema3E-Plexin-D1 signaling are intermingled with normal cells, the contribution of cells
134 lacking Sema3E-Plexin-D1 signaling to the tip cell population was predicted to increase

135 to 68-74% (robustly across a range of parameter values: $\delta = 4-6$, $s = 2-4$) in comparison to
136 control cells (Figure 2A,B, Video 8), with an increased speed of patterning compared to a
137 vessel entirely lacking Sema3E-Plexin-D1 signaling. This result suggests that normally,
138 Plexin-D1 cell-autonomously suppresses the tip cell phenotype.

139

140

141 To test the direct competition of *Plxnd1*^{-/-} cells and wildtype cells *in vivo*, we performed
142 mosaic analysis using mice with tamoxifen inducible loss of *Plxnd1* expression in the
143 vasculature (*Cdh5-Cre-ER*^{T2}; *Plxnd1*^{fllox/fllox}). In the sprouting front of the wildtype retina,
144 cells expressing Plexin-D1 were equally distributed at both tip cell and the adjacent stalk
145 cell positions (Figure 2C, left panel, Figure 2D), showing they have no preference for
146 either position. However, at approximately 45% of *Plxnd1*^{-/-} mosaicism, 75% of the
147 *Plxnd1*^{-/-} cells became tip cells (Figure 2C, middle panel, Figure 2D) indicating that these
148 cells do have a competitive advantage over Plexin-D1 expressing wildtype cells during
149 tip cell selection. In contrast, in control experiments using mice with tamoxifen inducible
150 expression of GFP (*Cdh5-Cre-ER*^{T2}; *Z/EG*⁺), GFP positive cells showed no preference
151 for either position (Figure 2C, right panel, Figure 2D), demonstrating that preferential tip
152 cell occupancy of mutant cells is due to lack of Sema3E-Plexin-D1 signaling. Taken
153 together, *in silico* prediction and *in vivo* mosaic retinal analyses demonstrate that
154 Sema3E-Plexin-D1 signaling suppresses the tip cell phenotype in a cell-autonomous
155 manner. Interestingly, this cell-autonomous effect at single cell level contrasts with the
156 effect of Sema3E-Plexin-D1 signaling at the collective level, where more new tip cells
157 are selected in the presence than in the absence of Sema3E-Plexin-D1 signaling (Figure
158 1). This finding highlights the differences between collective and cell autonomous
159 behaviors, and the challenge of intuiting one from the other.

160

161 Having confirmed that the calibrated set of parameters is valid to model contributions of
162 the Sema3E-Plexin-D1 pathway to VEGF/Notch patterning and to predict new *in vivo*
163 data of a static nature, we next employed the model to predict the effect of Sema3E-
164 Plexin-D1 signaling on the rate of tip cell selection during the fuller dynamic network
165 formation processes in which tip and stalk cell identities are constantly re-defined during

166 cell rearrangement/position switching. Here, we used a new “MSM-CPM” model that has
167 been previously extended, parameterized and experimentally validated to simulate
168 tip/stalk patterning together with cellular rearrangements within a vascular sprout
169 (Bentley et al., 2014a). In this model, a cell can move within the adhered collective of the
170 sprout powered by multiple local junctional movements. By incorporating the newly
171 calibrated Sema3E-PlexinD1 signaling extension the MSM-CPM model we simulated
172 cell rearrangements in vascular sprouts in the presence or absence of Sema3E-Plexin-D1
173 signaling (Figure 3A, B, Video 9,10). Simulations predicted that in the presence of
174 Sema3E-Plexin-D1 signaling, the tip cell is repeatedly overtaken by another cell. In
175 contrast, in the absence of Sema3E-Plexin-D1 signaling, tip cell overtaking frequency is
176 reduced by factor of 1.26; a given tip cell occupies the tip cell position for a longer time
177 (Figure 3C). Given the MSM is a qualitative not quantitative model we also performed
178 simulations over a range of parameters and found that if the strength of Dll4 upregulation
179 by VEGF (δ) is increased then this delay in overtaking is further exaggerated; a given tip
180 cell occupies the tip cell position longer (Figure 3C).

181

182 To test experimentally if tip cell selection and overtaking rates are slowed down in the
183 absence of Sema3E-Plexin-D1 signaling, we next performed live endothelial cell tracking
184 to follow the behavior of individual cells in an actively forming vascular network.
185 Previously, live imaging with single cell resolution has mainly been described in
186 sprouting assays using aortic rings (Arima et al., 2011) or embryoid bodies (EBs)
187 generated from ES cells (Jakobsson et al., 2010). However, those assays primarily give
188 rise to simple linear sprouts with less frequent branching than observed during retinal
189 angiogenesis. To better mimic *in vivo* temporal and spatial events within a highly
190 branched network, we developed a new *ex vivo* system, using explants from embryonic
191 lungs. Whole embryonic lungs (E12.0) were embedded within a collagen matrix in a
192 tissue culture dish containing medium supplemented with recombinant human VEGF.
193 After one day, endothelial sprouts grow out of the explant (Figure 4 – figure supplement
194 1A) with tip cells extending filopodia into the collagen matrix (Figure 4 – figure
195 supplement 1B). We observed branching events at various positions of the sprouts
196 (Figure 4B), as well as anastomosis (Figure 4 – figure supplement 1C), showing that all

197 steps of the *in vivo* angiogenic sprouting process are recapitulated in our system even
198 though there is no gradient of VEGF signaling. Lung explants endogenously express
199 *Sema3e* and *Plxnd1* (Figure 4 – figure supplement 1D). We could also detect Plexin-D1
200 and Dll4 in sprouting endothelial cells (Figure 4 – figure supplement 1 E, F). We next
201 performed long-term live imaging of wildtype and *Plxnd1*^{-/-} explants and analyzed tip cell
202 selection frequency. In contrast to the computational model where a tip cell selection
203 event can only occur via a switch between two cells at the tip of the sprout (Figure 3A),
204 in the live imaging assay, tip cell selection events occur in the following distinct
205 categories (Figure 4A, B): a positional switch between a tip and a stalk cell in a linear
206 sprout (switch), the selection of a new tip cell at the front of the sprout (branch, type I) or
207 at more proximal sites (branch, type II). Single cells were tracked manually using a
208 nuclear live stain. Consistent with the computational model prediction, *in vivo* live
209 imaging data indeed showed a significant delay in the selection of new tip cells in
210 *Plxnd1*^{-/-} vascular sprouts compared to wildtype sprouts. The overall appearance of new
211 tip cells, i.e. the tip cell selection frequency, was slowed down by factor 1.5 in the
212 mutants (Figure 4C, D, Video 11,12). When analyzing the different categories separately,
213 the number of events per total imaging time was significantly reduced in the categories
214 “switch” and “branch, type II” in the absence of Sema3E-Plexin-D1 signaling (Figure
215 4E).

216

217 Finally, to directly test experimentally whether the reduced tip cell selection rate
218 observed by live imaging in our *Plxnd1*^{-/-} lung explant indeed leads to a less branched
219 network over time, we analyzed the topology of the lung explant under the same culture
220 conditions as the live imaging paradigm. Using a computational method (Figure 4 –
221 figure supplement 2 and detailed description in the material and methods section) to
222 analyze the number of branching points in an unbiased way we found a significant
223 reduction in branching points of the network (Figure 4F, G). These data further
224 demonstrate that a slowed tip cell selection rate results in a less branched vascular
225 network.

226

227 Together, the *ex vivo* and *in silico* results demonstrate that Sema3E-Plexin-D1 signaling
228 modulate the pace of tip cell selection. In the absence of Sema3E-Plexin-D1 signaling,
229 the rate of tip cell selection is reduced, which overall leads to longer linear sprout
230 extension with less frequent branching substantially influencing the architecture of the
231 growing vasculature and resulting in a less dense network, as seen in the *Plxnd1* and
232 *Sema3e* mutant lung explant as well as in retina (Kim et al., 2011).

233

234 During angiogenesis, the topology of the network is shaped essentially through the
235 dynamic process of stalk cells turning into a new tip cell (tip cell selection), which is
236 dependent on the Delta-Notch lateral inhibition pathway, a widely used machinery to
237 regulate aspects of development that require temporal control by a “molecular clock”. For
238 example, during somitogenesis, Delta-Notch oscillations determine the frequency of new
239 somite formation (“the somite clock”) (Aulehla and Pourquié, 2008). In endothelial cells,
240 we propose that modulation of any of the components of the central pattern generator will
241 result in an altered pace of Delta-notch oscillations and an altered vascular patterning.
242 Deceleration of the Delta-notch feedback loop (by a “slow molecular metronome”) will
243 lead to the selection of fewer tip cells within a certain time frame and thus to the
244 formation of a less dense network with bigger pore sizes. Acceleration of the selection
245 process (by a “fast molecular metronome”) would result in an overly dense network
246 (Figure 4 – figure supplement 3). However, complex nonlinear feedback dynamics are
247 often hard to intuit, and further careful simulation integrated with experimentation will be
248 required to fully elucidate the temporal modulations and topological outcomes possible.

249

250 In this work, we describe how Sema3E-Plexin-D1 signaling can modify vascular density
251 by impinging on the central pattern generator VEGF/Notch signaling. Our computational
252 modeling predictions, mouse genetics mosaic analysis, and live imaging of individual cell
253 dynamics in actively forming blood vessel networks and computational quantification of
254 branching points show that the lack of Sema3E-Plexin-D1 signaling slows down the rate
255 of tip cell selection and rearrangement, resulting in a less branched vascular network.
256 Therefore, the Sema3E-Plexin-D1 pathway represents a “faster molecular metronome”
257 that results in a relatively dense network. These data suggest that *temporal* regulation of

258 this critical, iterative aspect of network formation could be a general mechanism, and
259 additional temporal regulators with varying pace (fast vs. slow) may exist to sculpt
260 vascular topology in different tissues. Furthermore, our findings may provide insights
261 into our understanding of morphogenesis in general, and aid in efforts to develop
262 therapeutic approaches for tissue engineering and control of tumor progression and
263 vascular diseases.

264

265 **Material and Methods.**

266

267 **Animals.** *Plxnd1^{fllox/fllox}* mice (Zhang et al., 2009), *Plxnd1^{+/-}* mice (Gu et al., 2005) and
268 *Cdh5-Cre-ER^{T2}* mice (Monvoisin et al., 2006) were maintained on a C57Bl/6
269 background. *Z/EG+* reporter (Novak et al., 2000) mice were maintained on a
270 129P3J;C57Bl/6 mixed background. Pregnant mice were obtained following overnight
271 mating (day of vaginal plug was defined as embryonic day 0.5). All animals were treated
272 according to institutional and US National Institutes of Health (NIH) guidelines approved
273 by the Institutional Animal Care and Use Committee (IACUC) at Harvard Medical
274 School.

275

276 **Mosaic retina analysis.** Cre-mediated recombination was induced by intraperitoneal
277 injection of tamoxifen (T5648, Sigma-Aldrich) dissolved in safflower oil on postnatal
278 day (P) 4. Due to the different Cre sensitivities at *Plxnd1* and *Z/EG* locus, we
279 experimentally determined the dosage of tamoxifen necessary for 45% of mosaicism. 25
280 pg of tamoxifen was injected in *Cdh5-Cre-ER^{T2}; Plxnd1^{fllox/fllox}* pups, and 10 ng of
281 tamoxifen was injected in *Cdh5-Cre-ER^{T2}; Z/EG+* pups. Mice were sacrificed at P5 and
282 retinas were isolated for analysis. *In situ* hybridization, Isolectin B4 staining and ERG
283 immunohistochemistry (1:200; SC353, Santa Cruz) were performed as described
284 previously. Images of flat mounted retinas were taken at 40x magnification using Zeiss
285 LSM 510 META confocal microscope. Images were processed using Adobe Photoshop[®]
286 and Image J (National Institutes of Health). Mosaic recombination in *Cdh5-Cre-*
287 *ER^{T2};Plxnd1^{fllox/fllox}* or *Z/EG; Cdh5-Cre-ER^{T2}* was analyzed by *Plxnd1* *in situ* signal or GFP
288 positivity, respectively, in combination with Isolectin B4 and endothelial nuclear ERG
289 staining. The tip cells were determined as blind-ended endothelial cells that are

290 associated with filopodia protrusions at the sprouting front. Endothelial cells (either tip or
291 stalk cells) were counted by combination of Erg positive staining and morphological
292 definition. 84 endothelial cells from 3 *Cdh5-Cre-ER^{T2};Plxnd1^{flox/flox}* animals and 64
293 endothelial cells from 3 wildtype animals were counted for tip cells and stalk cells that
294 were either *Plxnd1* positive or negative. 37 endothelial cells from 2 *Z/EG;Cdh5-Cre-ER^{T2}*
295 animals were counted for tip cells and stalk cells that were either GFP positive or
296 negative. Statistical significance was tested using two-way Anova.

297

298 **RT-PCR.** Total RNA was extracted from collagen embedded lung explants, or whole
299 retina using the RNeasy Micro Plus RNA extraction kit (Qiagen) according to
300 manufacturer's instructions. cDNA was generated from 100 ng total RNA using the
301 Superscript III reverse transcription kit (Invitrogen). The following primers were used to
302 detect *Plxnd1* and *Sema3e* transcripts: *Sema3e* forward 5'-aggctacgctgtcacataaa-3',
303 *Sema3e* reverse 5'-ccgttcttgatactcatccagc-3'; *Plxnd1* forward 5'-gctgactgtagcctatgggga-
304 3',*Plxnd1* reverse 5'- gccatctggtgggatgcat-3'.

305

306 ***Ex vivo* endothelial cell tracking assay.** Lungs were dissected from E12.0 embryos in
307 ice-cold dissecting medium (DMEM + Penicillin/Streptomycin), divided into single
308 lobes, washed in dissecting medium (30 min, 4°C) and embedded in a glass-bottom dish
309 (Mattek) between two layers of polymerized collagen IA gel (1.5 mg/ml, Cellmatrix)
310 prepared as previously described(Jakobsson et al., 2006). After solidification of collagen
311 (30 min, 37°C), imaging medium was added (DMEM without phenol red, 15% ES cell
312 grade FBS, 30 ng/ml rhVEGF (R&D systems), antibiotics). Explants were grown
313 overnight at 37°C, 5% CO₂. Next day, nuclear live stain solution (NucBlue, Life
314 Technologies) was added (2 drops/ml for 45 min). Imaging medium was replaced and
315 explants were imaged immediately using a Leica SP8 confocal microscope equipped with
316 a Tokai Hit chamber (37°C, 5% CO₂). 70 μm stacks were acquired at 20x magnification
317 every 10 minutes. Single cells were tracked manually using a combination of nuclear
318 staining and bright-field images of the sprouts. Per explant, 1-4 sprouts were analyzed for
319 9-20 hrs. Tip cell selection frequency was calculated as selection events observed per
320 hour live imaging. All 3 types of tip cell selection events were considered for

321 quantification of selection frequency. Statistical significance was tested using a
322 permutation test with shuffled genotypes.

323

324 **Immunostaining of lung explants.** Explants were dissected at E12.0 or E13.5, prepared
325 as described above, and fixed on day 2 or 3 in 4% PFA for 1 hr at RT. Then they were
326 washed in PBS (3x 10 min), permeabilized in blocking solution (PBS + 2% BSA + 0.2%
327 Triton) for 1 hr at RT (2x 30 min) and incubated with PECAM (1:300, BD), Plexin-D1
328 (abcam) or Dll4 (R&D) primary antibody in PBS + 0.2% Triton overnight at 4°C and
329 additional 6 hrs at RT. Explants were then washed in PBS + 0.1% Triton (6x 30 min),
330 incubated with secondary antibody in PBS + 0.1% Triton overnight at 4°C and washed in
331 PBS + 0.1% Triton (2x 30 min). If HRP-conjugated secondary antibody was used,
332 explants were washed longer (3x 30 min in PBS) and stained with DAB staining solution
333 (1 mg/ml Diaminobenzidine tetrahydrochloride in PBS, Sigma) for 3 min. For network
334 topology analysis, Alexa488 conjugated secondary antibody was used and explants were
335 imaged at a Leica SP8 confocal microscope at 10x magnification.

336

337 **Computational Modeling.** In the previously established “MemAgent-Spring Model”
338 (MSM) each endothelial cell is comprised of multiple smaller computational elements
339 (“agents”) that represent local sections of cell membrane and actin tension beneath. The
340 memAgents have dynamic internal levels of proteins, which enable them to sense protein
341 levels in the local extracellular environment (primarily VEGF ligands). The endothelial
342 cell integrates this local spatial information to determine its behavior (e.g. extension of
343 filopodia) and perform genetic regulatory processes (e.g. Dll4-Notch) after a time delay
344 representing the processes of transcription and translation (parameters D1 and D2 in
345 Figure 1B). As the time delay for Notch/VEGF gene expression is not currently known in
346 the mouse, the model was calibrated to match the known Notch periodicity (30 minutes)
347 of the zebrafish somite clock (Guidicelli and Lewis, 2004) so $D1=D2=28$ time steps
348 (representing 7 minutes of real time) as it was previously shown that, consistent with
349 period/delay relations in the Notch somite clock models (Guidicelli and Lewis, 2004), the
350 periodicity of Notch/VEGF signaling in the MSM model = $2 \times (D1+D2+R1+R2)$, where

351 R1 and R2 are the recovery delays, representing degradation rates, which were both set to
352 1 (Bentley et. al., 2008).

353

354 To include Sema3E-Plexin-D1 interactions to the existing MSM model of
355 VEGF/Notch/Dll4 signaling in endothelial cells during tip/stalk selection (full model
356 described in (Bentley et al., 2009, 2008)), four new parameters were included. Two new
357 time delay parameters: D3 controls how long it takes for VEGFR-2 to increase Plexin-D1
358 protein levels at the membrane and D4 determines the time it takes for an active Plexin-
359 D1 receptor to lower Dll4 expression. Additionally s was added to determine the strength
360 of Plexin-D1 down-regulation of Dll4 (specifically how many fewer Dll4 are produced
361 for one active Plexin-D1 receptor) and $r3$, which controls how long the down regulation
362 effect lasts for, encompassing the factors such as Plexin-D1 degradation rate, see Figure
363 1B for schematic.

364

365 As Sema3E is assumed to be uniformly present around the cell based on experimental
366 data in the mouse retina (Kim et al., 2011), activation of Plexin-D1 by Sema3E is not
367 directly modeled, but simply assumed to occur at a constant level. As the exact number
368 of Plexin-D1 receptors on the cell surface is also not known we assume Plexin-D1
369 receptors vary within the same range as VEGFR-2 receptors (see (Bentley et al., 2008)
370 for details), and are instantly activated by Sema3E when present. These assumptions
371 produce the most parsimonious model possible, permitting Plexin-D1 levels to be
372 controlled by just the D3 time delay parameter, and Sema3E-Plexin-D1 signaling strength
373 to be determined by the modulation of a single parameter s , which varies the strength of
374 effect of the signaling on Dll4 up-regulation specifically. Dll4 levels were then
375 determined as follows:

$$Dll4_{t+1} = Dll4_t + V''\delta - P''s$$

376 where V'' is the number of active VEGFR-2 receptors by VEGF after time delay D1 has
377 been applied, representing the current active VEGFR-2 level affecting gene expression in
378 the nucleus. Likewise P'' is the number of Plexin-D1 receptors (assumed activated by
379 Sema3E) able to affect gene expression after time delay D4.

380

381 Calibrating Dll4 regulation parameters δ, s

382 Previously δ , which represents the up-regulation strength of Dll4 by VEGF-VEGFR-2
383 signaling, was calibrated to 2 to generate matching tip/stalk pattern selection and
384 sprouting behavior *in vivo* under different conditions (Bentley et al., 2009, 2008). So now
385 with a balancing inhibition term s representing reduction in Dll4 via Plexin-D1, we know
386 that $\delta - s = 2$ is required for normal sprouting. Any combination of δ and s values such
387 that this relation held true would give normal sprouting. To simulate loss of Sema3E-
388 Plexin-D1 signaling s was set to zero. Thus the value for δ chosen ultimately determines
389 the strength of the simulated Sema3E-Plexin-D1 mutant phenotype, hence results are
390 shown throughout across a range of δ values when $s = 0$. For control simulations $s = \delta - 2$.

391

392 Calibrating time delay parameters D3 and D4

393 Experiments indicate that the rate of Plexin-D1 up-regulation by pVEGFR-2 is fast
394 compared to pVEGFR-2 up-regulation of Dll4, indicating that together the delays $D3 + D4$
395 $\geq D1$. To investigate the effects of varying the temporal regulation of Plexin-D1 on tip
396 cell selection a sensitivity analysis was performed simulating with different delay settings
397 for the new parameters D3 and D4 (a full analysis of varying delays D1 and D2 is given
398 in (Bentley et al., 2008)). It was found that the lateral inhibition mechanism is strictly
399 sensitive to the values of these new delay parameters relative to the existing delays D1
400 and D1. In the model, only a setting of $D3 + D4 = D1$ would allow for normal tip cell
401 selection in control conditions (Video 1). Even a delay with D3 or D4 $\neq \pm 1$ timestep in
402 the model (representing 15 seconds) would disrupt the process and tip cells could not be
403 selected and the system falls into unrealistic “flashing” oscillations as the cells instantly
404 raise and then lower *dll4* each time step through the Notch/VEGF negative feedback loop
405 resulting in a counter intuitive hypersprouting rather than inhibited phenotype as no cell
406 is under the inhibition long enough to become a stalk cell (Video 2, 3). Interestingly if all
407 delay parameters are set to zero, representing the null hypothesis that no time delays are
408 required to explain the phenotype, the same system behavior occurs as in Video 2 and 3
409 illustrating the importance of explicitly representing the amount of time that gene
410 expression takes in computational models.

411

412

413 Calibrating the degradation rate r_3

414 Disrupting the degradation rate r_3 of Plexin-D1 was also found to have drastic effects on
415 the ability of the system to select tip cells. The r_3 parameter was required to satisfy: $r_3 =$
416 $r_2 = r_1 = 1$ timestep (representing 15 seconds). Any increase led to similar irregular
417 flashing oscillations and abrogated tip cell selection as seen with increases to the delays
418 D3 or D4 (Video 4 and 5). Thus for all simulations $D_3 + D_4 = D_1$, where $D_3 = 1$ and $D_4 =$
419 27 timesteps.

420

421 Mosaic vessel simulations

422 Mosaic vessels follow the same simulation method as simulations of a fully wildtype or
423 mutant vessel, except that at the start of the simulation each cell is randomly assigned a
424 wildtype or mutant setting of the δ and s parameters (Video 8). 45% mosaicism was
425 calculated as average of simulations with 40% and 50% mosaicism. Results were
426 averaged over 50 runs.

427

428 The “MSM-CPM” model

429 In this model a cell can move within the adhered collective of the sprout powered by
430 multiple local junctional adhesion movements (based on the Cellular Potts Model “CPM”
431 of differential adhesion (Graner and Glazier, 1992)), which are regulated by VEGF/Notch
432 signaling.

433

434 **Computational method used for vascular network analysis.** The stacks were
435 processed and analyzed in 3D using the following Python 2.7 modules: Numpy, Scipy,
436 Matplotlib, Opencv2, Igraph and Networkx.

437

438 The first step of the algorithm was to apply a Gaussian smoothing filter to the stacks. A
439 standard deviation of 5 μm was used for the Gaussian kernel. Next, the moment-
440 preserving threshold technique (Tsai, 1985) was used in order to find a proper threshold
441 for stack binarization. Pixels having intensity values larger than the calculated threshold
442 were classified as belonging to a vessel. Remaining image components (Stockman, and

443 Shapiro, 2001) smaller than $20000 \mu\text{m}^3$ were considered background noise and removed
444 from the binary image. A thinning procedure (Palagyi and Kuba, 1998) was then applied
445 to the binary image, resulting in what we call the skeleton (Costa and Jr, 2009) of the
446 blood vessels. The skeleton tends to present some sets of connected pixels having more
447 than two neighbors each. Such sets were erased from the skeleton and represented as a
448 single pixel at the center of mass of the set. The remaining skeleton pixels having at least
449 three neighbors were classified as branching points, while pixels having one neighbor
450 were considered a termination point.

451

452 Spurious skeleton segments were removed by an iterative algorithm. First, termination
453 segments smaller than $20 \mu\text{m}$ were erased, where a termination segment is defined as a
454 segment having one termination point. After erasing such segments, new small
455 termination segments might appear. They were iteratively erased until no new
456 termination segments smaller than $20 \mu\text{m}$ remained. The sample was then characterized
457 by quantification of the remaining branching points. Finally, in order to validate the
458 analysis, we created images containing both the original image and the final skeletons
459 and verified that the obtained skeletons were accurately representing the original blood
460 vessel structure. Statistical significance was tested using a permutation test with shuffled
461 genotypes.

462

463 **Acknowledgements.**

464 We thank Drs. Christopher Harvey, Jonathan Cohen, Ayal Ben-Zvi, and members of the
465 Gu laboratory for comments on the manuscript. We thank Dr. Christopher Harvey for
466 statistical analysis, and Rob Rosa for technical help on lung explant imaging. We thank
467 S. Demaki for providing the *Z/EG+* reporter mice, Tom Jessell for providing
468 *Plxnd1^{fllox/flox}* mice, Luisa Iruela-Arispe for providing the *Cdh5-Cre-ER^{T2}* mice. The
469 Enhanced Neuroimaging Core at Harvard Neurodiscovery Center for help with imaging
470 and advice on image analysis. This work was supported by: DFG-German Research
471 Foundation postdoctoral fellowship KU 3081/1&2 (E.K.); NRSA Postdoctoral training
472 grant T32 NS07484-12 (J.K.); Brooks postdoctoral fellowship (A.T.); FAPESP grants
473 11/22639-8 (C.H.C.) and 11/50761-2 (L.daF.C.) and CNPq grant 307333/2013-2

474 (L.daF.C.); BIDMC and the Leducq transatlantic Network ARTEMIS (K.B.); and the
475 flowing grants to C.G.: NIH grants R01NS064583, DP1 NS092473, the BrightFocus
476 Foundation, and a Kaneb Fellowship.

477

478 **References**

- 479 Adams, R.H., Eichmann, A., 2010. Axon guidance molecules in vascular patterning. *Cold*
480 *Spring Harb. Perspect. Biol.* 2, a001875. doi:10.1101/cshperspect.a001875
- 481 Arima, S., Nishiyama, K., Ko, T., Arima, Y., Hakozaki, Y., Sugihara, K., Koseki, H.,
482 Uchijima, Y., Kurihara, Y., Kurihara, H., 2011. Angiogenic morphogenesis
483 driven by dynamic and heterogeneous collective endothelial cell movement. *Dev.*
484 *Camb. Engl.* 138, 4763–4776. doi:10.1242/dev.068023
- 485 Aulehla, A., Pourquié, O., 2008. Oscillating signaling pathways during embryonic
486 development. *Curr. Opin. Cell Biol.* 20, 632–637. doi:10.1016/j.ceb.2008.09.002
- 487 Benedito, R., Roca, C., Sörensen, I., Adams, S., Gossler, A., Fruttiger, M., Adams, R.H.,
488 2009. The notch ligands Dll4 and Jagged1 have opposing effects on angiogenesis.
489 *Cell* 137, 1124–1135. doi:10.1016/j.cell.2009.03.025
- 490 Bentley, K., Franco, C.A., Philippides, A., Blanco, R., Dierkes, M., Gebala, V., Stanchi,
491 F., Jones, M., Aspalter, I.M., Cagna, G., Weström, S., Claesson-Welsh, L.,
492 Vestweber, D., Gerhardt, H., 2014a. The role of differential VE-cadherin
493 dynamics in cell rearrangement during angiogenesis. *Nat. Cell Biol.* 16, 309–321.
494 doi:10.1038/ncb2926
- 495 Bentley, K., Gerhardt, H., Bates, P.A., 2008. Agent-based simulation of notch-mediated
496 tip cell selection in angiogenic sprout initialisation. *J. Theor. Biol.* 250, 25–36.
497 doi:10.1016/j.jtbi.2007.09.015
- 498 Bentley, K., Harrington, K.I., Regan, E.R., 2014b. In Can active perception generate
499 bistability? Heterogeneous collective dynamics and vascular patterning. *ALIFE*
500 14 Fourteenth Int. Conf. Synth. Simul. Living Syst. 14, 328–335.
- 501 Bentley, K., Mariggi, G., Gerhardt, H., Bates, P.A., 2009. Tipping the balance: robustness
502 of tip cell selection, migration and fusion in angiogenesis. *PLoS Comput. Biol.* 5,
503 e1000549. doi:10.1371/journal.pcbi.1000549
- 504 Bentley, K., Philippides, A., Ravasz Regan, E., 2014c. Do endothelial cells dream of
505 eclectic shape? *Dev. Cell* 29, 146–158. doi:10.1016/j.devcel.2014.03.019
- 506 Carmeliet, P., 2000. Mechanisms of angiogenesis and arteriogenesis. *Nat. Med.* 6, 389–
507 395. doi:10.1038/74651
- 508 Costa, L. da F., Jr, R.M.C., 2009. *Shape Classification and Analysis: Theory and*
509 *Practice.* CRC Press, Inc.
- 510 Fukushima, Y., Okada, M., Kataoka, H., Hirashima, M., Yoshida, Y., Mann, F., Gomi,
511 F., Nishida, K., Nishikawa, S.-I., Uemura, A., 2011. Sema3E-PlexinD1 signaling
512 selectively suppresses disoriented angiogenesis in ischemic retinopathy in mice. *J.*
513 *Clin. Invest.* 121, 1974–1985. doi:10.1172/JCI44900
- 514 Gerhardt, H., Golding, M., Fruttiger, M., Ruhrberg, C., Lundkvist, A., Abramsson, A.,
515 Jeltsch, M., Mitchell, C., Alitalo, K., Shima, D., Betsholtz, C., 2003. VEGF
516 guides angiogenic sprouting utilizing endothelial tip cell filopodia. *J. Cell Biol.*
517 161, 1163–1177. doi:10.1083/jcb.200302047

518 Graner, null, Glazier, null, 1992. Simulation of biological cell sorting using a two-
519 dimensional extended Potts model. *Phys. Rev. Lett.* 69, 2013–2016.

520 Guarani, V., Deflorian, G., Franco, C.A., Krüger, M., Phng, L.-K., Bentley, K.,
521 Toussaint, L., Dequiedt, F., Mostoslavsky, R., Schmidt, M.H.H., Zimmermann,
522 B., Brandes, R.P., Mione, M., Westphal, C.H., Braun, T., Zeiher, A.M., Gerhardt,
523 H., Dimmeler, S., Potente, M., 2011. Acetylation-dependent regulation of
524 endothelial Notch signalling by the SIRT1 deacetylase. *Nature* 473, 234–238.
525 doi:10.1038/nature09917

526 Guidicelli, F., Lewis, J., 2004. The vertebrate segmentation clock. *Curr. Opin. Genet.*
527 *Dev.* 14, 407–14.

528

529 Hellström, M., Phng, L.-K., Hofmann, J.J., Wallgard, E., Coultas, L., Lindblom, P., Alva,
530 J., Nilsson, A.-K., Karlsson, L., Gaiano, N., Yoon, K., Rossant, J., Iruela-Arispe,
531 M.L., Kalén, M., Gerhardt, H., Betsholtz, C., 2007. Dll4 signalling through
532 Notch1 regulates formation of tip cells during angiogenesis. *Nature* 445, 776–780.
533 doi:10.1038/nature05571

534 Jakobsson, L., Franco, C.A., Bentley, K., Collins, R.T., Ponsioen, B., Aspalter, I.M.,
535 Rosewell, I., Busse, M., Thurston, G., Medvinsky, A., Schulte-Merker, S.,
536 Gerhardt, H., 2010. Endothelial cells dynamically compete for the tip cell position
537 during angiogenic sprouting. *Nat. Cell Biol.* 12, 943–953. doi:10.1038/ncb2103

538 Jakobsson, L., Kreuger, J., Holmborn, K., Lundin, L., Eriksson, I., Kjellén, L., Claesson-
539 Welsh, L., 2006. Heparan sulfate in trans potentiates VEGFR-mediated
540 angiogenesis. *Dev. Cell* 10, 625–634. doi:10.1016/j.devcel.2006.03.009

541 Kim, J., Oh, W.-J., Gaiano, N., Yoshida, Y., Gu, C., 2011. Semaphorin 3E-Plexin-D1
542 signaling regulates VEGF function in developmental angiogenesis via a feedback
543 mechanism. *Genes Dev.* 25, 1399–1411. doi:10.1101/gad.2042011

544 Kurz, H., Gärtner, T., Eggli, P.S., Christ, B., 1996. First blood vessels in the avian neural
545 tube are formed by a combination of dorsal angioblast immigration and ventral
546 sprouting of endothelial cells. *Dev. Biol.* 173, 133–147.
547 doi:10.1006/dbio.1996.0012

548 Leslie, J.D., Ariza-McNaughton, L., Bermange, A.L., McAdow, R., Johnson, S.L.,
549 Lewis, J., 2007. Endothelial signalling by the Notch ligand Delta-like 4 restricts
550 angiogenesis. *Dev. Camb. Engl.* 134, 839–844. doi:10.1242/dev.003244

551 Lobov, I.B., Renard, R.A., Papadopoulos, N., Gale, N.W., Thurston, G., Yancopoulos,
552 G.D., Wiegand, S.J., 2007. Delta-like ligand 4 (Dll4) is induced by VEGF as a
553 negative regulator of angiogenic sprouting. *Proc. Natl. Acad. Sci. U. S. A.* 104,
554 3219–3224. doi:10.1073/pnas.0611206104

555 Monvoisin, A., Alva, J.A., Hofmann, J.J., Zovein, A.C., Lane, T.F., Iruela-Arispe, M.L.,
556 2006. VE-cadherin-CreERT2 transgenic mouse: a model for inducible
557 recombination in the endothelium. *Dev. Dyn. Off. Publ. Am. Assoc. Anat.* 235,
558 3413–3422. doi:10.1002/dvdy.20982

559 Novak, A., Guo, C., Yang, W., Nagy, A., Lobe, C.G., 2000. Z/EG, a double reporter
560 mouse line that expresses enhanced green fluorescent protein upon Cre-mediated
561 excision. *Genes. N. Y. N* 2000 28, 147–155.

562 Palagyi, K., Kuba, A., 1998. A 3D 6-subiteration thinning algorithm for extracting medial
563 lines. *Pattern Recogn Lett* 19, 613–627.

564 Phng, L.-K., Potente, M., Leslie, J.D., Babbage, J., Nyqvist, D., Lobov, I., Ondr, J.K.,
565 Rao, S., Lang, R.A., Thurston, G., Gerhardt, H., 2009. Nrarp coordinates
566 endothelial Notch and Wnt signaling to control vessel density in angiogenesis.
567 Dev. Cell 16, 70–82. doi:10.1016/j.devcel.2008.12.009
568 Roca, C., Adams, R.H., 2007. Regulation of vascular morphogenesis by Notch signaling.
569 Genes Dev. 21, 2511–2524. doi:10.1101/gad.1589207
570 Stockman, G.C., Shapiro, L.G., 2001. Computer Vision. Prentice Hall.
571 Suchting, S., Freitas, C., le Noble, F., Benedito, R., Bréant, C., Duarte, A., Eichmann, A.,
572 2007. The Notch ligand Delta-like 4 negatively regulates endothelial tip cell
573 formation and vessel branching. Proc. Natl. Acad. Sci. U. S. A. 104, 3225–3230.
574 doi:10.1073/pnas.0611177104
575 Tsai, W.H., 1985. Moment-preserving thresholding: A new approach. Comput. Vis.
576 Graph. Image Process. 29, 377–393.
577 Zhang, Y., Singh, M.K., Degenhardt, K.R., Lu, M.M., Bennett, J., Yoshida, Y., Epstein,
578 J.A., 2009. Tie2Cre-mediated inactivation of plexinD1 results in congenital heart,
579 vascular and skeletal defects. Dev. Biol. 325, 82–93.
580 doi:10.1016/j.ydbio.2008.09.031
581

582 **Figure Legend.**

583 **Figure 1. Calibrated computational model predicts delayed tip cell selection in the**
584 **absence of Sema3E-Plexin-D1 signaling. A,** Whole-mount vascular staining (Isolectin
585 B4) of retinas from *Sema3e*^{-/-} and wildtype littermates at P4. The mutant vasculature
586 exhibits a reduced number of tip cells and branching points (asterisks) and an uneven
587 growth front (arrows and arrowheads). Scale bar: 500 μ m. **B,** Feedback between the
588 VEGF/Notch and Sema3E-Plexin-D1 signaling pathways included in the extended agent-
589 based computational model of tip cell selection. D1-D4: transcriptional delays. r1-r3:
590 recovery delays representing degradation. δ , s, σ : change in expression levels in response
591 to receptor activation. **C,** Simulated tip cell selection. Colors represent Dll4 levels on a
592 continuum from purple (low) to green (high). The red boxes highlight a time frame in
593 which a salt and pepper pattern has formed in the control vessel, while in the absence of
594 Sema3E-Plexin-D1 signaling, only few early tip cells have been selected. **D,** Average
595 number of selected tip cells in simulated vessels. At a timepoint where the simulated
596 control vessel (black line) already exhibits an alternating pattern of tip and stalk cells, the
597 simulated vessel lacking Sema3E-Plexin-D1 signaling (blue line, for a given set of
598 parameter values: $\delta = 5$, s=3) shows a 50% reduction in tip cells. Thin lines: standard
599 deviation. n=50. **E,** *In silico* Dll4 levels in single endothelial cells during simulated tip

600 cell selection. In the control situation (top), Dll4 levels quickly stabilize. In the absence
601 of Sema3E-Plexin-D1 signaling (bottom) Dll4 levels fluctuate in near synchrony before
602 they finally stabilize.

603 **Figure 2. Sema3E-PlexinD1 signaling is cell-autonomously required to suppress tip**
604 **cell identity. A,** Simulated tip cell selection in a mosaic vessel with 50% mutant cells
605 placed randomly. Cells without Sema3E-Plexin-D1 signaling are indicated by bright pink
606 color, which turns to yellow if Dll4 levels increase. For wildtype cells: purple = low Dll4,
607 pink = high Dll4. **B,** Comparison of simulated and *in vivo* contribution to the tip cell
608 population by cells lacking Sema3E-Plexin-D1 signaling at 45% mosaicism. A range of δ
609 values simulates different strengths of loss of Sema3E-Plexin-D1 signaling. Simulations,
610 $n=50$, *in vivo*, $n=6$. Data is represented as mean \pm SEM. **C,** Analysis of the occupation
611 of tip or stalk cell position by *Plxnd1* expressing wildtype cells in control retina (left),
612 and *Plxnd1*^{-/-} cells (middle) or GFP+ cells (right) in mosaic retinas at P5. Red: vascular
613 membrane staining (Isolectin B4), blue: vascular nuclear staining (α -ERG), green: *Plxnd1*
614 *in situ* hybridization (left, middle), α -GFP staining (right). **D,** Quantification of c. n.s.=
615 not significant, ** $p=0.0033$. WT retinas, $n=6$; *Plxnd1*^{-/-} mosaic retinas, $n=6$; GFP+
616 mosaic retinas, $n=4$. Scale bar: 50 μ m. Data is represented as mean \pm SEM.

617

618 **Figure 3. Computational simulation predicts that lack of Sema3E-Plexin-D1**
619 **signaling leads to prolonged tip cell occupancy and reduced tip cell overtaking**
620 **frequency. A,** Single frames of cell rearrangements in simulated sprouts of 10 cells.
621 VEGF gradient extends in direction of vessel. **B,** Kymograph plots of cell rearrangements
622 in simulated sprouts. Each line represents one endothelial cell. Arrows indicate
623 overtaking events at the tip cell position in a and b. **C,** Quantification of overtaking
624 events at the tip cell position in the presence and absence of Sema3E-Plexin-D1
625 signaling. A range of δ values simulates different strengths of loss of Sema3E-Plexin-D1
626 signaling. The setting $\delta=5$, which matched loss of Sema3E-Plexin-D1 signaling in other
627 conditions in the paper exhibits a 1.26 slower tip cell overtaking frequency (events/hour.) As
628 δ increases there is a clear trend towards slower tip cell overtaking across δ values. Data is
629 presented as mean \pm SD, $n=50$.

630 **Figure 4. Endothelial cell live tracking in ex vivo lung explants reveals a reduction**
631 **in tip cell selection frequency and a less branched lung vascular network in the**
632 **absence of Sema3E-Plexin-D1 signaling. A,** Different types of tip cell selection events
633 observed during live imaging. **B,** Single frames from live imaging experiments
634 illustrating the different types of tip cell selection events. Arrowheads point out the newly
635 selected tip cells. Nuclei: blue. Scale bar: 50 μ m. **C,** Long-term live imaging experiments
636 of vascular sprouts from wildtype and *Plxnd1*^{-/-} lung explants. Single planes from z-
637 stacks are shown. Arrowheads indicate a tip cell selection event. Nuclei: blue (top and
638 middle), white (bottom). Individual nuclei are outlined by different colors in the middle
639 panel. **D,** Quantification of tip cell selection frequency calculated as events per hour. Tip
640 cell selection frequency is reduced by factor 1.5 in sprouts from *Plxnd1*^{-/-} explants. WT,
641 n=24 sprouts from 12 explants. *Plxnd1*^{-/-}, n=30 sprouts from 11 explants. Data is
642 represented as mean +/- SEM. **E,** Quantification of tip cell selection frequency calculated
643 as incidence of events in each category as illustrated in (a) during total imaging time.
644 **p=0.013 (d), *p=0.029 (e ‘switch’), 0.041 (e ‘branch, type II’), permutation test with
645 shuffled genotypes. **F,** Vascular sprouts originating from *Plxnd1*^{+/-} and *Plxnd1*^{-/-} lung
646 explants on day 3. Left: whole-mount vascular staining (green, PECAM), right:
647 reconstructed/skeletonized network, Scale bar: 250 μ m. **G,** Quantification of branching
648 points per area. The number of branching points is significantly reduced in *Plxnd1*^{-/-} lung
649 explants. Data is represented as mean +/- SEM. *Plxnd1*^{+/-}, n=7 explants; *Plxnd1*^{-/-}, n=6
650 explants. ***p=0.0005, permutation test with shuffled genotypes.

651 **Figure 4 – figure supplement 1: The ex vivo sprouting assay. A,** Sprouts originating
652 from the lung explant express endothelial specific marker PECAM. Explants at day 1
653 (left) and day 3 (right) are shown. Scale bar: 300 μ m. **B,** Tip cells extend filopodia
654 (arrows) into the collagen matrix. Scale bar: 50 μ m. **C,** Anastomosis: a new connection
655 (arrow) is formed between neighboring sprouts. Scale bar: 50 μ m **D,** *Sema3e* and *Plxnd1*
656 are expressed by embryonic lung explants as shown by RT PCR. **E,** Sprouting endothelial
657 cells express Plexin-D1 (green). PECAM staining shown in red. Scale bar: 10 μ m. **F,** In
658 wildtype endothelial sprout Dll4 (green) localized in the tip cells (arrow). Dll4-positive
659 area is increased in *Plxnd1*^{-/-} explants. Scale bar: 10 μ m.

660 **Figure 4 – figure supplement 2: Computational method used for vascular network**
661 **analysis.** The region of interest (ROI) was defined as the vascular network originating
662 from the lung explants. Vasculature inside the lung tissue was excluded from the
663 analysis. Stacks of confocal images were binarized and then skeletonized by thinning.
664 Branching points were identified as skeleton pixels with at least three neighbors and
665 quantified to characterize the vascular network. The 2D images shown are the maximum
666 intensity z-projections of the original 3D stacks, except for the binary image, which is an
667 intensity sum z-projection.

668

669 **Figure 4 – figure supplement 3: Model: Modifications of the central pattern**
670 **generator lead to the formation of diverse vascular topologies.** The unique topologies
671 of organ-specific vascular networks are dependent on the tight temporal control of the tip
672 cell selection process. The VEGF-Notch lateral inhibition pathway is the central pattern
673 generator of tip cell selection. We suggest that in different tissues, specific target-derived
674 signals functioning as “molecular metronomes” regulate the pace of the pattern generator
675 to ensure the formation of networks that cater each tissue’s specific need. A “fast
676 molecular metronome” (e.g. Sema3E-Plexin-D1 signaling) will speed up the Dll4/Notch
677 feedback loop and increase the frequency of tip cell selection, leading to the formation of
678 a dense network with a small pore size, while a “slow molecular metronome” will slow
679 down the Dll4/Notch feedback loop and decrease the tip cell selection frequency,
680 resulting in a network with larger pore sizes.

681 **Video legend**

682 **Video 1:** Calibration of time delay parameters (induction of Plexin-D1, reduction of Dll4
683 levels). Simulation of tip cell selection with Sema3E-Plexin-D1 related regulatory time
684 delays equal to the time it takes for pVEGFR-2 to up-regulate Dll4 ($D3+D4=D1$). Color
685 indicates cell Dll4 levels (green = high, purple = low).

686

687 **Video 2:** Calibration of time delay parameters (induction of Plexin-D1, reduction of Dll4
688 levels). Simulation of tip cell selection with Sema3E-Plexin-D1 related regulatory time
689 delays slightly slower than the time it takes for pVEGFR-2 to up-regulate Dll4

690 (D3+D4=D1+1). Dll4 levels flash irregularly between very high and very low with no
691 stable selection possible. Color indicates cell Dll4 levels (green = high, purple = low).

692

693 **Video 3:** Calibration of time delay parameters (induction of Plexin-D1, reduction of Dll4
694 levels). Simulation of tip cell selection with Sema3E-Plexin-D1 related regulatory time
695 delays slightly faster than the time it takes for pVEGFR-2 to up-regulate Dll4
696 (D3+D4=D1-1). Dll4 levels flash irregularly between very high and very low with no
697 stable selection possible. Color indicates cell Dll4 levels (green = high, purple = low).

698

699 **Video 4:** Calibration of Plexin-D1 degradation rate. Simulation of tip cell selection with
700 slowed degradation of Plexin-D1 allowing it to affect transcription of Dll4 for one
701 timestep (12 seconds) longer. Dll4 levels flash irregularly between very high and very
702 low with no stable selection possible. Color indicates cell Dll4 levels (green = high,
703 purple = low).

704

705 **Video 5:** Calibration of Plexin-D1 degradation rate. Simulation of tip cell selection with
706 slowed degradation of Plexin-D1 allowing it to affect transcription of Dll4 for two
707 timesteps (30 seconds) longer. Dll4 levels flash irregularly between very high and very
708 low with no stable selection possible. Color indicates cell Dll4 levels (green = high,
709 purple = low).

710

711 **Video 6:** Simulation of a vessel with 20 endothelial cells in the absence of Sema3E-
712 Plexin-D1 signaling. Extended regions occur with no sprouting as cells battle for longer
713 undergoing fluctuations as the Dll4 up-regulation is higher. These eventually resolve and
714 tip cells are selected across the whole region.

715

716 **Video 7:** Simulation of a wildtype vessel for comparison with Video 7. The selection
717 occurs much faster and more regularly than in the vessel without Sema3E-Plexin-D1
718 signaling.

719

720 **Video 8:** Simulated mosaic vessel with 50% mutant cells placed randomly. Cells without
721 Sema3E-Plexin-D1 signaling are indicated by bright pink color, which turns to yellow if
722 Dll4 levels increase. For wildtype cells: purple = low Dll4, pink = high Dll4 as before.
723 This chimera achieves a 75% contribution of mutant cells to the tip.

724

725 **Video 9:** Simulation of normal cell rearrangement and tip cell overtaking in a sprout
726 consisting of ten cells, two per vessel cross section. VEGF gradient extends in the
727 direction of the sprout. Each cell indicated by a different color.

728 **Video 10:** Simulation of cell rearrangement in a sprout, in the absence of Sema3E-
729 Plexin-D1, consisting of ten cells, two per vessel cross-section. VEGF gradient extends in
730 the direction of the sprout. Each cell indicated by a different color.

731 **Video 11:** Wildtype sprout in *ex vivo* endothelial cell tracking assay. The movie
732 represents 9 hours of live imaging and corresponds to Figure 4C, left panel. Merge of
733 fluorescent channel (nuclear live stain) and brightfield channel. Arrows indicate newly
734 selected tip cells that give rise to a new sprout. Arrowhead indicates a switching event.
735 Single planes from z-stacks are shown.

736 **Video 12:** *Plxnd1*^{-/-} sprout in *ex vivo* endothelial cell tracking assay. The movie
737 represents 9 hours of live imaging and corresponds to Figure 4C, right panel. Merge of
738 fluorescent channel (nuclear live stain) and brightfield channel. Arrows indicate newly
739 selected tip cells that give rise to a new sprout. Single planes from z-stacks are shown.

740

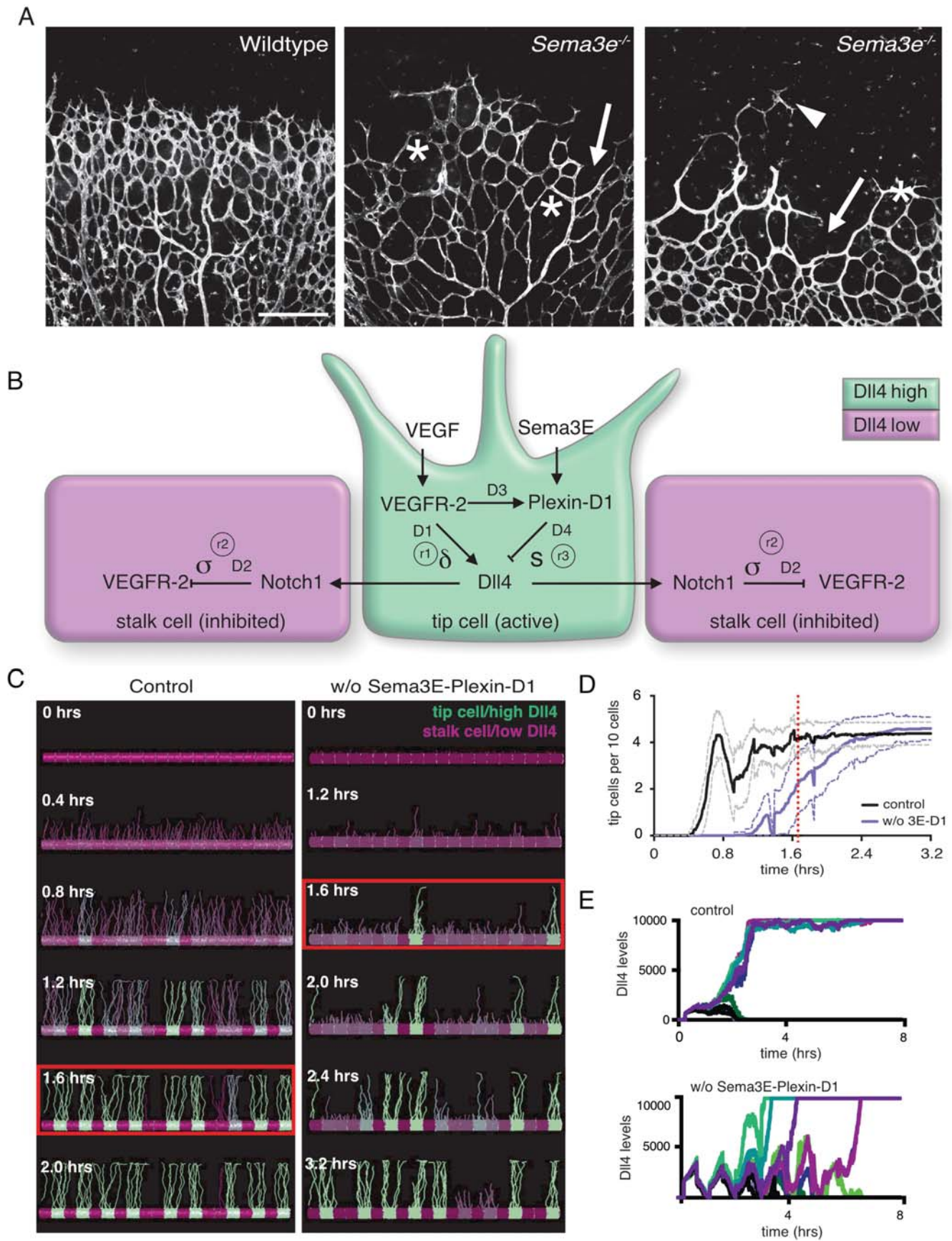


Figure 1

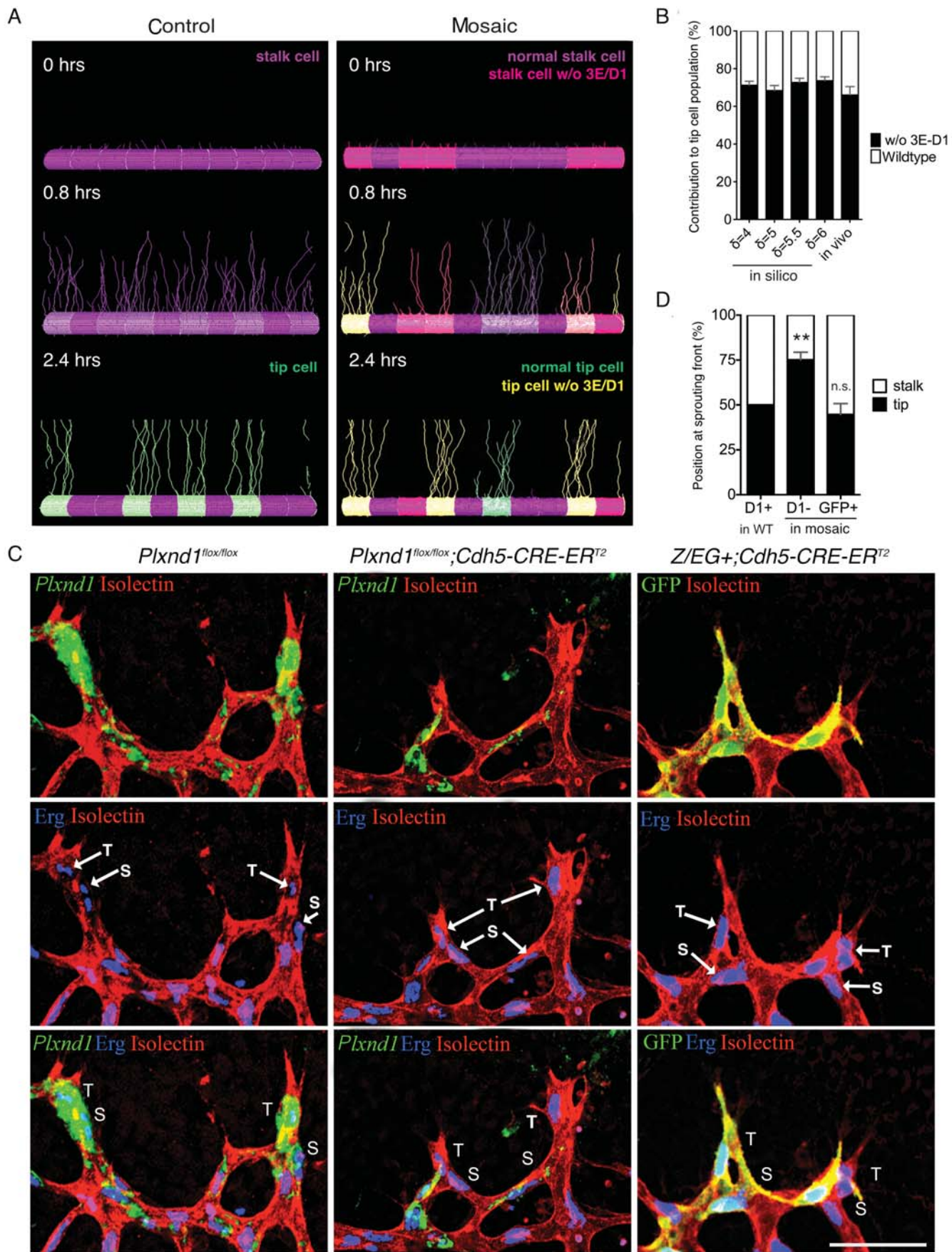


Figure 2

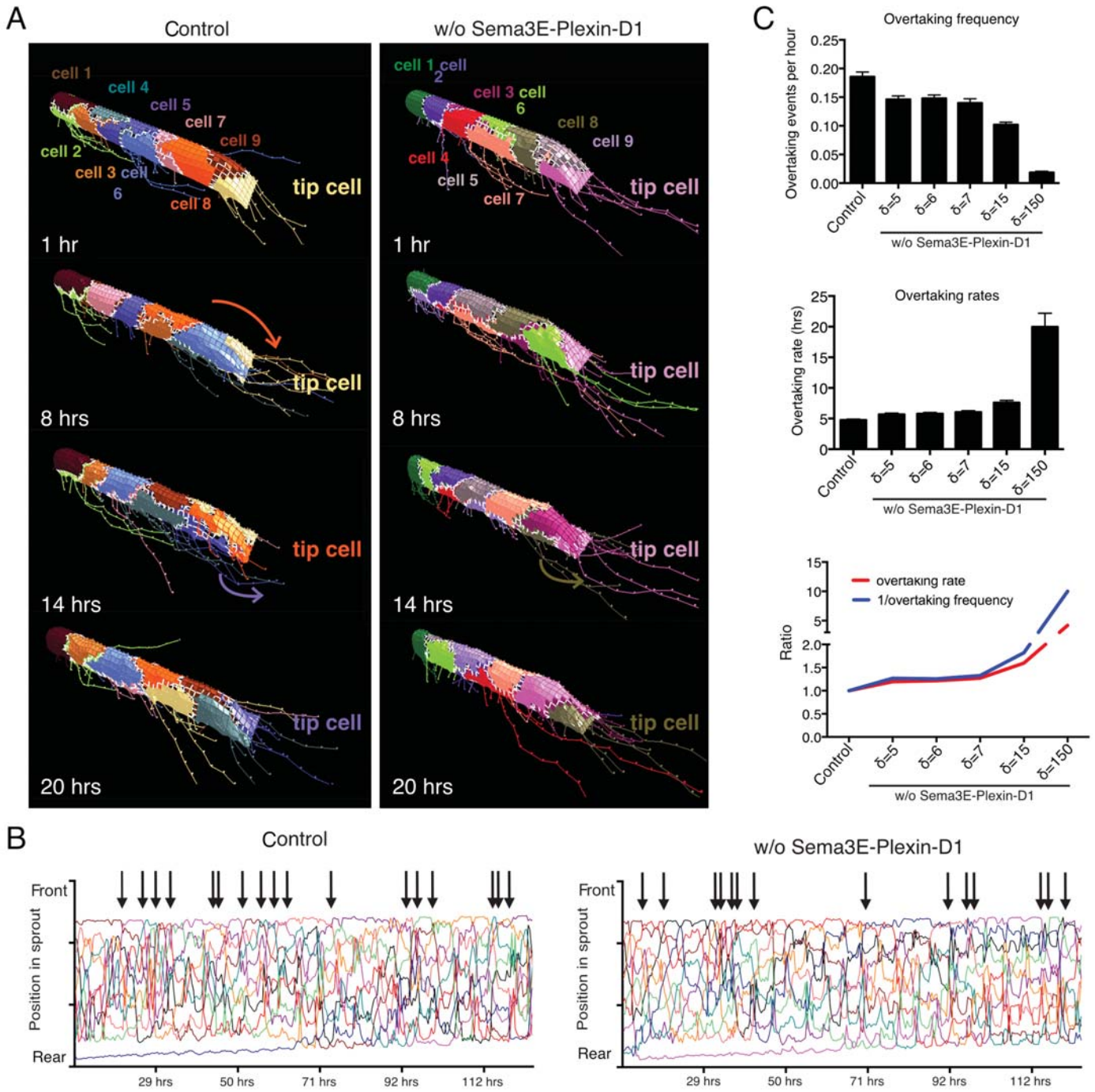


Figure 3

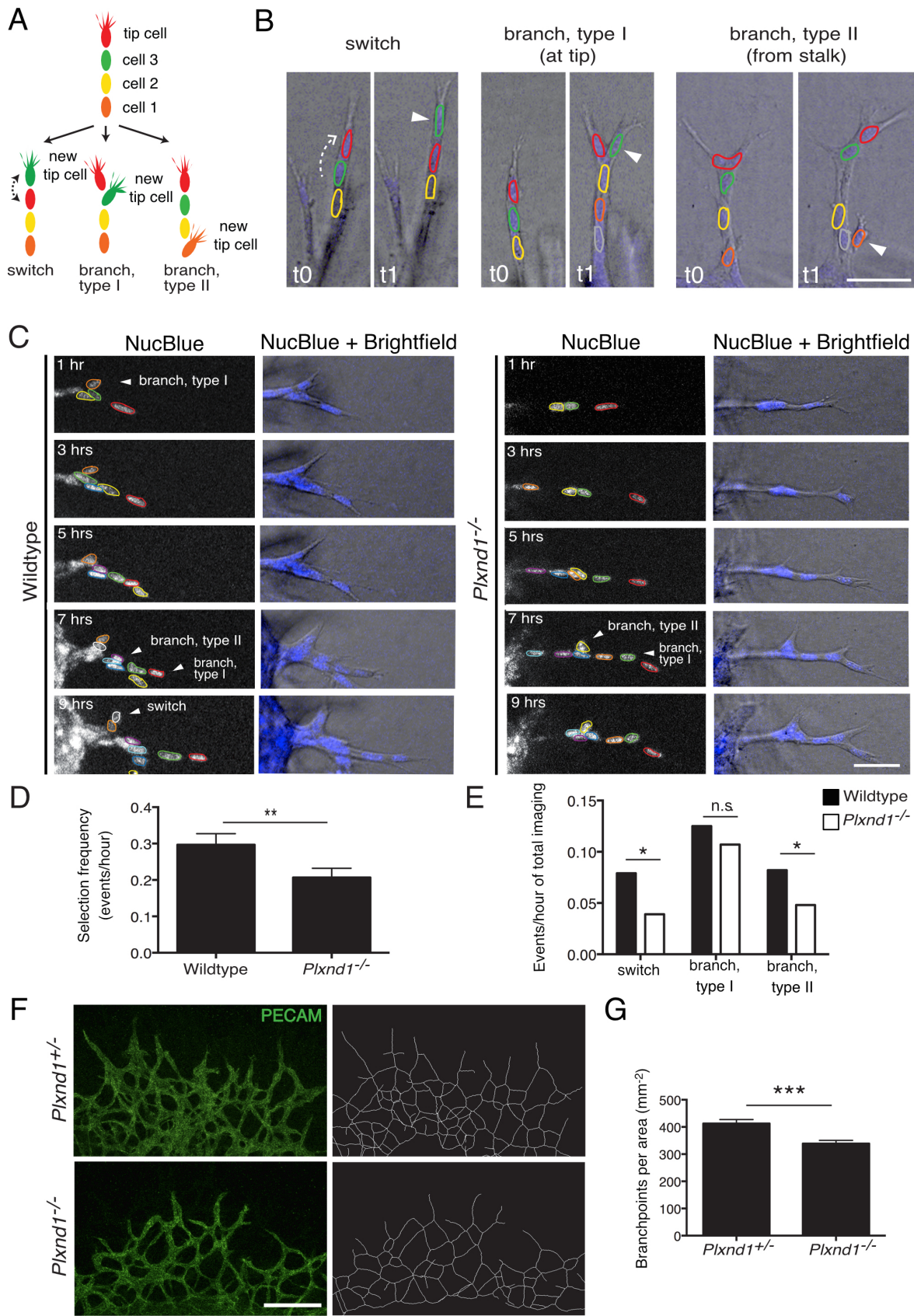


Figure 4